A novel statistical analysis of chloropigment fluxes to constrain particle exchange and organic matter remineralization rate constants in the Mediterranean Sea

Wei-Lei Wang[a,b,*], Cindy Lee[a], J. Kirk Cochran[a], François W. Primeau[b], Robert A. Armstrong[a]

[a] School of Marine and Atmospheric Sciences, Stony Brook University, Stony Brook, NY 11794-5000, USA
[b] Department of Earth System Science, University of California at Irvine, Irvine, CA 92697, USA

ARTICLE INFO

ABSTRACT

To investigate particle dynamics, we used a 3-prong modeling approach. First we constructed a conceptual finite difference (FD) model to describe chloropigment and organic matter (OM) cycling. Second, from the FD model, we obtained a set of synthetic data; we then used Bayesian techniques to recover parameters used in the FD model to show that Bayesian techniques have the ability to make parameter estimations. Third, we built a two-layer model and applied the Bayesian approach to the data from Indented Rotating Sphere (IRS) sediment traps operating in Settling Velocity (SV) mode to estimate particle and pigment cycling rate constants. Eleven settling velocity categories collected by SV sediment traps were grouped into two sinking velocity classes (fast-sinking and slow-sinking classes) to decrease the number of parameters that needed to be estimated, with a fast/slow cutoff SV of 49 m/d adopted from previous work. The organic matter degradation rate constant was estimated to be $1.5_{-0.4}^{+0.5}\,y^{-1}$, which is equivalent to a degradation half-life of ~0.5 years. The rate constant of chlorophyll a degradation to pheopigments (sum of pheophorbide, pheophytin, and pyropheophorbide) was estimated to be $1.6_{-0.3}^{+0.4}\,y^{-1}$, pheopigment remineralization was $2.1_{-0.5}^{+0.7}\,y^{-1}$, both of which are higher than the organic matter degradation rate constant. Disaggregation/aggregation rate constants were $149.9_{-99.6}^{+297.3}\,y^{-1}$ and $3.2_{-2.4}^{+9.9}\,y^{-1}$, respectively. We compare our data with previously published thorium-based particle aggregation and disaggregation rate constants at this site and consider how this comparison can be used to explore particle exchange concepts.

1. Introduction

Sinking particles play a pivotal role in the oceanic biological pump by transferring photosynthesized products and energy from the euphotic zone into the deep ocean (McCave, 1975; Honjo, 1980). However, the transfer efficiency is low. Only a small portion of organic matter produced by photosynthesis in the surface layer survives transit through the water column to the deep ocean and sea floor (Lee and Wakeham, 1988). Particle sinking velocity, a factor that controls particle residence time, plays an important role in regulating transfer efficiency. Larger, denser particles sink faster than smaller, lighter particles, but aggregation of smaller particles into larger particles leads to increased transfer efficiency.

The extent to which particles aggregate and disaggregate has been estimated with radiochemical tracers, such as the naturally occurring thorium isotopes (e.g., Nozaki et al., 1987; Murnane et al., 1990, 1994; Clegg et al., 1991; Cochran et al., 1993, 2000). However, parameters estimated using radionuclides sometimes have wide ranges. This variation might be caused by spatial, seasonal, and/or other variability. For comparison purposes and to further investigate particle exchange processes, here we applied a Bayesian method to chloropigment tracers instead of radioisotopes to estimate particle interaction/respiration rate constants. In contrast to radionuclides, pigment tracers are an integral part of the organic matter in particles produced in surface waters by phytoplankton; therefore, they may better represent particles being exported from the euphotic zone than radionuclides. On the other hand, pigment degradation rates are less well characterized than radionuclide decay. The large number of organic compounds found in sinking particles, many with different age and source, opens the possibility that the approach presented here can be used to look at different types of particles.

Chlorophyll a (Chl a), an important light absorber found in all phytoplankton, is produced only in the euphotic zone and undergoes degradation during particle transit from surface waters to the deep sea

(Lee et al., 2000). This degradation can be caused either by photolysis to colorless compounds, or by heterotrophic degradation to pheopigments (pheophorbide, pheophytin, and pyropheophorbide), which have ring structures similar to that of Chl *a*. Degradation pathways can be different for different heterotrophs in seawater (Szymczak-Zy la et al., 2008). Chl *a* is often used as a proxy for the biomass of algae, which are small in size and sink slowly. However, many of the pheopigments are products of herbivore grazing, and can be found inside zooplankton fecal pellets (Welschmeyer and Lorenzen, 1985), which can sink much faster in the water column than individual algal cells or small aggregates. During their transit through the water column, particles are thought to continuously exchange material through aggregation and disaggregation (e.g., Hill, 1998), although this may be a seasonally variable process (Abramson et al., 2010). Chl *a* and pheopigments can be useful proxies to record particle exchange, since they are present in different ratios in phytoplankton and fecal pellets.

The purpose of this paper is to use a novel modeling approach to determine aggregation and disaggregation rate constants and organic carbon degradation rate constants for individual compounds, using particulate pigment data as an example. The data were obtained in 2005 as part of the MedFlux Program (Lee et al., 2009a). The sampling site was the French JGOFS DYFAMED time-series site in the NW Mediterranean Sea. The present modeling study was motivated by our previous work using thorium to estimate rate constants of particle exchange (Wang et al., 2016), and by the findings of Abramson et al. (2010) on particle exchange. In the latter study, pigment compositions were compared between particles sampled using in-situ large volume pumps, which are assumed to sample both sinking and non-sinking particles indiscriminately, and particles sampled by Time Series (TS) sediment traps, which sample sinking particles. Abramson et al. (2010) showed that there were distinct differences in pigment composition between particles sampled by pumps and by sediment traps during the high-productivity spring bloom period, but that pigment composition differences became less apparent during the low-productivity summer period. These observations suggested that during the spring bloom, particle exchanges were limited, while during the low-productive summer period particle exchanges were extensive. However, Abramson et al. (2010) were not able to estimate quantitatively the rate at which particles exchange. In this paper, we examine particle exchange quantitatively by estimating particle exchange rate constants. Rather than using TS sediment trap (separating particles by time) and pump data, the present paper uses settling velocity (SV) (separating particles by sinking velocity) sediment trap data, which include pigment and organic matter fluxes collected in eleven settling velocity ranges. We will compare aggregation and disaggregation rates with values obtained previously using radioisotope data from the same samples (Wang et al., 2016).

2. Methods

2.1. MedFlux data collection

Sinking particles were collected using Indented Rotating Sphere (IRS) SV sediment traps, which were deployed at the French JGOFS DYFAMED site (43°20′ N, 7°40′ E) during March 4 to April 28, 2005 (Lee et al., 2009a). The sampling site, though only 53 km off the coast of Nice in the Ligurian Sea, has many open-ocean characteristics because most terrestrial influence is cut off by the alongshore Ligurian current (Marty, 2002). As a site located in the mid-latitude northern hemisphere, it experiences a phytoplankton spring bloom from March to April followed by a period of low primary production in summer. The decrease in stratification in autumn promotes another, smaller phytoplankton bloom, which is terminated by decreased temperature and intensified mixing in winter.

The IRS sediment trap was originally invented to exclude swimmers (Peterson et al., 1993); this innovation was later exploited to allow the trap to sort sinking particles based on particle settling velocity, as described in Peterson et al. (2005, 2009). Generally, sinking particles are first caught by a cylindrical particle interceptor and then deposited on an indented sphere that is programmed to rotate. The rotation of the ball dumps the particles into a skewed funnel that leads to a 12-chamber sampling carousel. Eleven sampling tubes are filled with filtered seawater collected at trap depths, and HgCl$_2$ is added to the tubes to prevent heterotrophic decomposition. The first sampling chamber in the carousel is an open drain so that no sample is lost from an open tube during trap deployment and recovery. Different rotation schedules of the rotating sphere and of the sampling carousel can separate particles based on either collection date (time-series [TS] mode) or particle settling velocity (SV mode).

Total particulate organic carbon (TPC) and particulate organic carbon (POC) data used in this modeling study are reported in Lee et al. (2009b) and Abramson et al. (2010). Chloropigment data are described in Wakeham et al. (2008) and Abramson et al. (2010).

2.2. Model description and development

Generally, this section is divided into three parts. First, we present a finite difference model used to conceptually describe organic matter and pigment cycles in the ocean, and to generate a set of synthetic data, which we contaminated with normally distributed errors. Second, we used the contaminated data to test if a new Bayesian approach can recover the true model parameter values. Third, we built a two-layer model and applied the Bayesian approach to the sediment trap flux data to estimate particle and pigment cycling rate constants. The first two steps describe and evaluate the model formulation, and the third step is an application of the model.

2.2.1. Conceptual finite difference model

To build a finite difference model, we divided the ocean into 24 vertical layers, with the upper-most layer having a thickness of 30 m, and deepening to 600 m for the deepest layer (the thickness of each layer are 30, 30, 40, 40, 60, 60, 80, 80, 80, 120, 120, 120, 120, 200, 200, 200, 200, 400, 400, 400, 400, 600, 600, 600 m). The cycling of organic matter and pigments in each layer is described in Fig. 1. The model formulation is based on the following assumptions.

1. Chl *a* appreciably degrades to pheopigments only in slow-sinking particles; both Chl *a* and organic matter degradation in fast-sinking particles are negligible due to their rapid transit through the water column.

2. The amount of Chl *a* lost by degradation is equal to the amount of pheopigment gained (Shuman and Lorenzen, 1975). More Chl *a* is lost than pheopigment gained during degradation in marine systems since Chl *a* also degrades to colorless products, so our Chl-*a* degradation rates are minimum values.

3. Particle aggregation, disaggregation, pigment degradation, and organic matter degradation follows first-order kinetics in agreement with Murnane et al. (1994, 1996) and Stephens et al. (1997). This is a commonly used assumption and the real reaction order is unknown; second-order reaction kinetics on particle aggregation is left for a future study.

The conceptual model shown in Fig. 1 describes the exchanges between fast- and slow-sinking classes through aggregation and disaggregation: slow-sinking particles can contribute to the mass of fast-sinking particles by aggregation; and fast-sinking particles can disaggregate to form slow-sinking particles. Pigments are exchanged between the two classes when bulk particle aggregation and disaggregation occur. Chl *a* in slow-sinking particles degrades into pheopigments. Organic matter and pheopigments in slow-sinking particles remineralize into inorganic carbon, with their own specific remineralization rate constants d_2 and d_3, respectively.
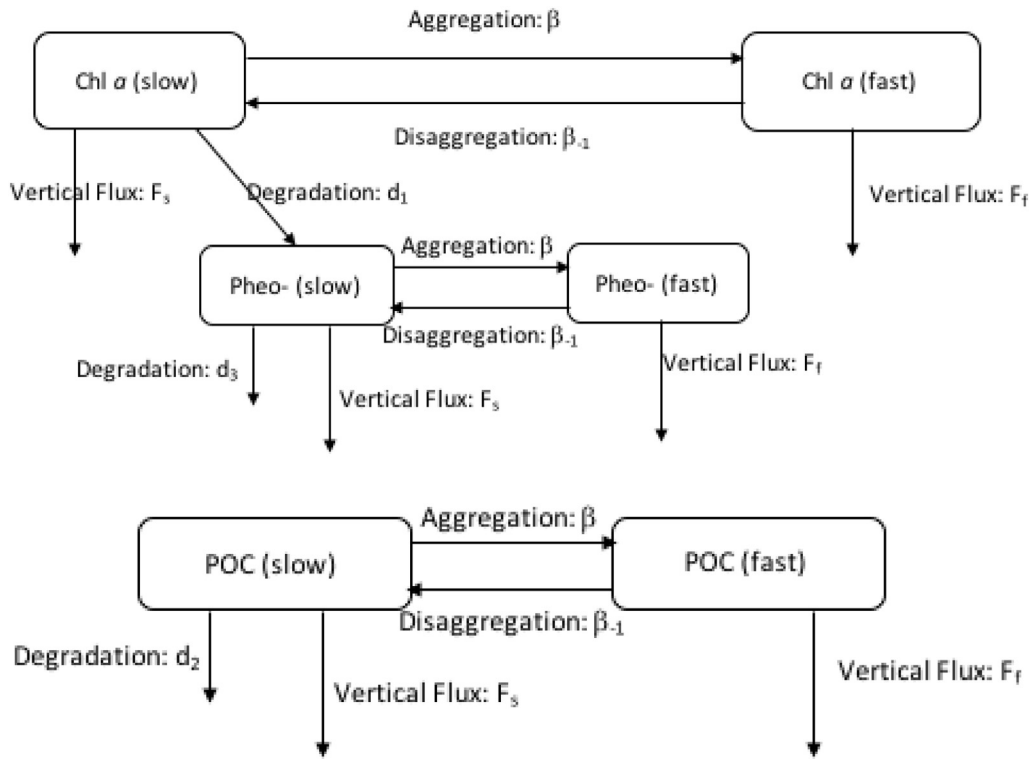
Fig. 1. A conceptual finite difference model describing particulate pigment cycling. Slower-sinking particles aggregate to form faster sinking particles, and faster-sinking particles disaggregate into slower sinking particles. Chl-*a* degradation products in slower-sinking particles have two sources: in-situ degradation of Chl *a* and disaggregation of faster-sinking particles containing the pheopigments. Chl *a* in faster-sinking particles can increase due to aggregation of slower-sinking particles, and can be lost by disaggregation. d1 is defined as the rate constant of Chl-*a* degradation into pheophorbide, pheophytin, and pyropheophorbide. d2 is defined as the degradation rate constant of organic matter. d_3 is defined as the degradation rate constant of chloropigments. Degradation loss of both Chl *a* and organic matter in faster-sinking particles is assumed to be slow enough to be neglected.

$$\frac{dP_s}{dt} = \beta_{-1}P_f - (\beta + d_2 + \mathbf{PFD}_s)P_s + P_{s0}$$

$$\frac{dP_f}{dt} = \beta P_s - (\beta_{-1} + \mathbf{PFD}_f)P_f + P_{f0}$$

$$\frac{dPh_s}{dt} = \beta_{-1}Ph_f - (\beta + d_3 + \mathbf{PFD}_s)Ph_s + d_1Chl_s + Ph_{s0}$$

$$\frac{dPh_f}{dt} = \beta Ph_s - (\beta_{-1} + \mathbf{PFD}_f)Ph_f + Ph_{f0}$$

$$\frac{dChl_s}{dt} = \beta_{-1}Chl_f - (\beta + d_1 + \mathbf{PFD}_s)Chl_s + Chl_{s0}$$

$$\frac{dChl_f}{dt} = \beta Chl_s - (\beta_{-1} + \mathbf{PFD}_f)Chl_f + Chl_{f0}$$

where P_s, P_f, Ph_s, Ph_f, Chl_s, and Chl_f are slow-, fast-sinking organic matter, pheopigments, and Chl-*a* concentrations, respectively. β and β_{-1} are particle aggregation and disaggregation rate constants, respectively, d_1 is Chl-*a* degradation to pheopigment rate constant, d_2 is organic matter respiration rate constant, and d_3 is a pheopigment respiration rate constant. $\mathbf{PFD}_s$ and $\mathbf{PFD}_f$ are particle flux divergence operators $\left(\mathbf{PFD}_c \equiv \frac{\omega(z)\partial C}{\partial z}\right.$, where C denotes particle/pigment concentration, z is depth, and ω is sinking speed), which were built based on the Martin curve (Kriest and Oschlies, 2008), for slow- and fast-sinking particles, respectively. The sinking speed is implicitly built into the particle flux divergence operators. To make the finite difference model work, we prescribed production rates for each component, P_{s0}, P_{f0}, Ph_{s0}, Ph_{f0}, Chl_{s0}, and Chl_{f0}, which are $N \times 1$ vectors (N is the number of grid layers), whose values in the surface three layers (mimicking euphotic zone 0–100 m) were approximated from SV sediment trap measurements at 313 m. We multiplied the measurements at 313 m by a factor

of four to compensate for remineralization between 100 and 313 m. Production rates below the euphotic zone are set to zero. Note that the production rates (measured value times a factor of four) only impact the synthetic data. They do not influence the parameter estimation in the two-layer model, which is designed to avoid prescription of productions as discussed in Section 2.2.3. The model was spun up to equilibrium. The resulting model-predicted particle and pigment distributions (idealized data) are shown in Fig. 2.

2.2.2. Bayesian approach to recovery of model parameters

To test the Bayesian method, we contaminated the idealized data with normally distributed errors with a mean of zero and variance of 0.05, 0.1 and 0.5. At steady state, the governing equation can be written in the following matrix form.

$$
\begin{pmatrix}
\beta\mathbf{I} + d_2\mathbf{I} & -\beta_{-1}\mathbf{I} & 0^*\mathbf{I} & 0^*\mathbf{I} & 0^*\mathbf{I} & 0^*\mathbf{I} \\
+ \mathbf{PFD}_s & & & & & \\
-\beta\mathbf{I} & \beta_{-1}\mathbf{I} + \mathbf{PFD}_f & 0^*\mathbf{I} & 0^*\mathbf{I} & 0^*\mathbf{I} & 0^*\mathbf{I} \\
0^*\mathbf{I} & 0^*\mathbf{I} & \beta I + d_3\mathbf{I} + \mathbf{PFD}_s & -\beta_{-1}\mathbf{I} & d_1\mathbf{I} & 0^*\mathbf{I} \\
0^*\mathbf{I} & 0^*\mathbf{I} & -\beta\mathbf{I} & \beta_{-1}\mathbf{I} + \mathbf{PFD}_f & 0^*\mathbf{I} & 0^*\mathbf{I} \\
0^*\mathbf{I} & 0^*\mathbf{I} & 0^*\mathbf{I} & 0^*\mathbf{I} & \beta\mathbf{I} + d_1\mathbf{I} + \mathbf{PFD}_s & -\beta_{-1}\mathbf{I} \\
0^*\mathbf{I} & 0^*\mathbf{I} & 0^*\mathbf{I} & 0^*\mathbf{I} & -\beta\mathbf{I} & \beta_{-1}\mathbf{I} + \mathbf{PFD}_f
\end{pmatrix}
$$

$$
\times
\begin{pmatrix}
P_s \\ P_f \\ Ph_s \\ Ph_f \\ Chl_s \\ Chl_f
\end{pmatrix}
=
\begin{pmatrix}
P_{s0} \\ P_{f0} \\ Ph_{s0} \\ Ph_{f0} \\ Chl_{s0} \\ Chl_{f0}
\end{pmatrix}
$$

,where $\mathbf{I}$ is a $N \times N$ identity matrix. Since the system is linear, the tracer concentrations (P_s, P_f, $\cdots Chl_f$) can be obtained by direct matrix inversion. The obtained tracer concentrations (model) were fit to the contaminated idealized data by optimizing a set of five parameters (β, β_{-1}, d_1, d_2, and d_3). To keep the rate constants positive, we did
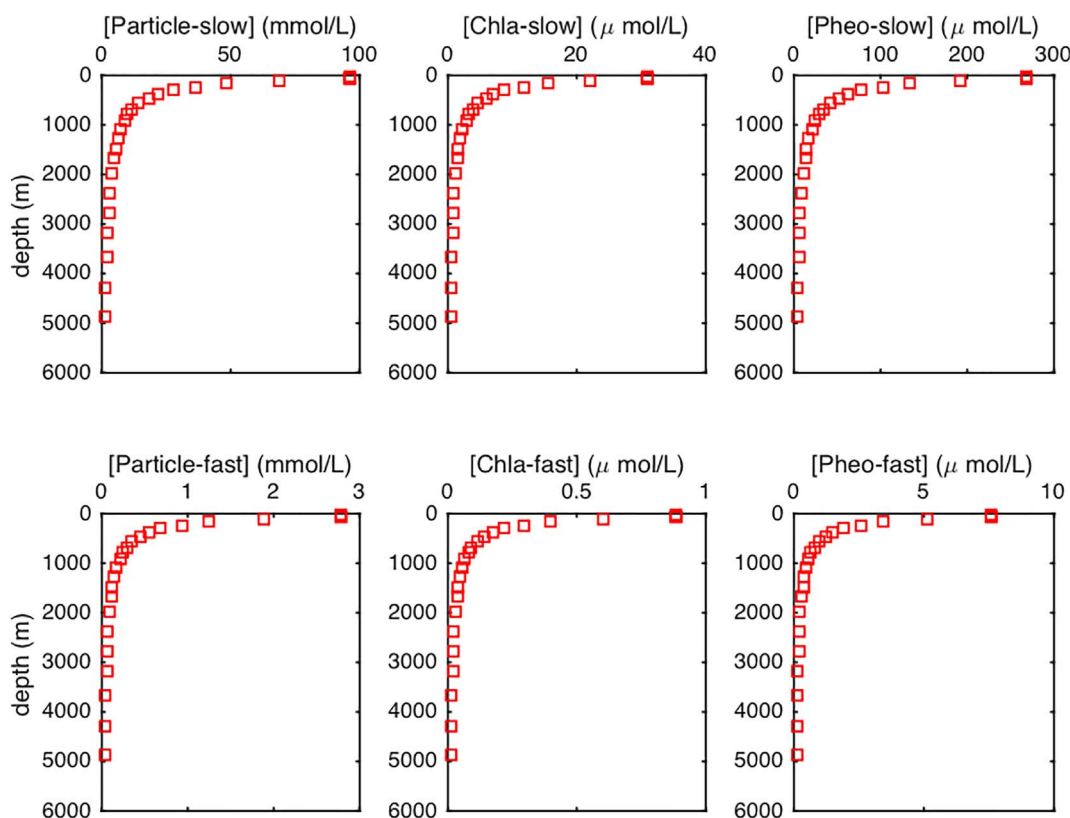
Fig. 2. POC and pigment depth distributions predicted by the finite difference model using parameters listed in Table 2.

lognormal transformation to the five parameters. The optimization was conducted using Matlab's built-in function *fminunc* to find the most probable parameter combination that makes the misfit between model and observation as small as possible. Parameter uncertainty estimations followed the method of Teng et al. (2014). The parameter Hessian matrix is associated with parameter covariance, and square roots of diagonal elements are the related parameter error bars (Sivia and Skilling, 2006).

2.2.3. The two-layer model

We then built a two-layer model to overcome the necessity of prescribing euphotic zone POC and pigment production, which in this study was not well known. The model's layer boundaries coincide with the depths of the sediment traps (313, 524, and 1918 m). To formulate the "two-layer" model, we made two additional assumptions over the time scale of sinking particles:

1. There is no primary production at our study depth, which is 313–1918 m. These trap depths are well below both the euphotic zone and the mixed layer at the DYFAMED station (Marty et al., 2002).
2. The system is at steady state. Very little in the ocean is at steady

state given daily, seasonal, and inter-annual variations, so our results must be considered averages over the sampling times, as are all previous modeling efforts of this sort.

Each layer in this model corresponds to the depth interval between two vertically aligned sediment traps. We assume that the flux in each layer changes linearly with depth, and that the flux at depth z can be expressed using fluxes measured at the top ($f_{i,top}$) and bottom ($f_{i,bot}$) of the layer according to:

$$f_{i,z} = \frac{(z_{bot} - z)f_{i,top} + (z - z_{top})f_{i,bot}}{z_{bot} - z_{top}} \tag{1}$$

where z_{top} and z_{bot} are depths of sediment traps at the top and bottom of the layer, respectively.

According to Armstrong et al. (2009), the concentration at depth z can be calculated by dividing the flux at depth z ($f_{i,z}$) by the corresponding category's geometric mean sinking velocity (SV_i) that was measured using the SV traps. Thus, concentration at depth z (C_z) is calculated using

$$C_{i,z} = \frac{(z_{bot} - z)C_{i,top} + (z - z_{top})C_{i,bot}}{z_{bot} - z_{top}} \tag{2}$$

Table 1
Parameters used in the finite difference (FD) model, and recovered using the Bayesian approach with error bars, which correspond to plus/minus one standard deviation of the posterior probability distribution. σ^2 is the variance of normally distributed error used to contaminate the synthetic data.

Parameters	FD model	Recovery I ($\sigma^2 = 0.05$)	Recovery II ($\sigma^2 = 0.1$)	Recovery III ($\sigma^2 = 0.5$)
Aggregation (β)	3	$2.9_{-0.1}^{+0.1}$	$2.7_{-0.3}^{+0.2}$	$3.8_{-0.3}^{+0.4}$
Disaggregation (β_{-1})	150	$147.8_{-2.8}^{+2.9}$	$144.3_{-5.25}^{+5.45}$	$139.8_{-12.0}^{+13.2}$
Chl a degradation (d_1)	1	$1.1_{-0.1}^{+0.1}$	$1.2_{-0.2}^{+0.2}$	$0.0_{-0.0}^{+Inf}$
OC degradation (d_2)	1	$1.0_{-0.1}^{+0.1}$	$1.2_{-0.2}^{+0.2}$	$0.8_{-0.3}^{+0.6}$
Pheo- degradation(d_3)	1	$1.1_{-0.1}^{+0.1}$	$1.2_{-0.2}^{+0.2}$	$0.6_{-0.3}^{+0.6}$

Table 2

Settling velocity fluxes (µg/m²/d) for 2005 of composite pigments and organic matter. In the 2005 deployment there were two SV traps at each depth. The data from two SV traps are combined via the following equation: $f_{composite} = SV1_{mass} / (SV1_{mass} + SV2_{mass}) \cdot SV1(f) + SV2_{mass} / (SV1_{mass} + SV2_{mass}) \cdot SV2(f)$. 'Pheopigments' is the sum of ppb, pyro and pptn in the model. The original data is available online at: http://www.somassbu. org/research/medflux/pages/datapub/2005/Moored_Sed_Traps.html

Geomean SV (m/d)	Composite Chl a (µg/m²/d)	Composite ppb[a] (µg/m²/d)	Composite pyro[a] (µg/m²/d)	Composite pptn[a] (µg/m²/d)	Composite OM (mg/m²/d)
Depth: 313 m					
1211.9	0.174	0.322	0.707	0.444	1.968
692.4	1.041	2.113	5.328	1.038	6.654
399.8	1.773	2.775	9.696	1.589	4.593
252.8	2.290	3.548	16.018	2.010	5.535
165.5	1.026	1.765	5.827	0.852	3.059
117.0	1.384	1.837	6.503	0.917	2.573
69.2	1.229	2.122	9.121	1.094	3.603
32.6	0.997	1.616	5.205	0.807	2.405
15.4	0.682	1.442	4.153	0.732	3.271
7.7	0.763	1.326	5.096	0.617	2.535
1.9	2.851	4.889	16.436	2.716	8.092
Depth: 524 m					
1211.9	2.469	1.653	5.377	0.491	2.971
692.4	1.728	2.941	6.550	3.992	8.053
399.8	1.334	1.801	5.889	0.710	3.798
252.8	1.447	2.883	7.974	1.351	3.560
165.5	0.561	1.006	3.902	0.596	1.755
117.0	0.749	1.059	2.527	0.650	1.506
69.2	0.631	1.032	2.235	0.449	1.496
32.6	0.568	0.966	2.259	0.482	1.624
15.4	0.447	0.784	2.455	0.394	1.641
7.7	0.666	1.224	4.436	0.618	2.763
1.9	2.123	4.400	8.878	2.342	6.533
Depth: 1918 m					
1211.9	0.154	0.177	0.934	0.389	0.844
692.4	1.616	2.593	6.729	2.046	4.262
399.8	0.874	1.623	2.717	1.002	3.120
252.8	1.121	2.161	4.561	1.536	3.052
165.5	0.547	1.000	2.614	0.572	1.642
117.0	0.519	0.892	2.840	0.444	0.988
69.2	0.463	0.872	2.883	0.777	1.603
32.6	0.283	0.546	1.656	0.499	0.990
15.4	0.218	0.343	1.352	0.434	0.812
7.7	0.313	0.397	1.217	0.214	1.158
1.9	0.874	1.489	5.175	1.102	3.103

[a] ppb is *pheophorbide*; pyro is *pyropheophorbide*; pptn is *pheophytin*.

where $C_{i,top}$ and $C_{i,bot}$ are POC or pigment concentration at the top and bottom boundary, respectively, in sinking velocity category i.

At steady state, flux change between the top and bottom boundaries is caused by the sum of interactions inside the layer:

$$\Delta f_i = \sum \left(\phi_{i,j} \right) \tag{3}$$

where $\Delta f_i = f_{i,top} - f_{i,bot}$, flux difference between the top and bottom of the studied layer. The data are summarized in Table 2, and full data set is available online at http://www.somassbu.org/research/medflux/. $\phi_{i,j}$ is the contribution of interaction j (degradation, aggregation, or disaggregation) for settling velocity category i. The contribution of a process to the flux change can be expressed using the following equation:

$$\varnothing_{i,j} = \int_{top}^{bot} (k_j C_{i,z}) dz = k_j \int_{top}^{bot} C_{i,z} dz \tag{4}$$

where k_j is the rate constant of interaction j (β, β_{-1}, d_1, d_2, and d_3, where applicable) and $C_{i,z}$ is the corresponding concentration (i) at depth z, which is calculated based on Eq. (2).

Since we adopt a cut-off SV of 49 m/d from Armstrong et al. (2009) to reduce the eleven sinking velocity categories to two sinking classes, the slow-sinking class contains four SV categories (0.68 m/d, 5.44 m/d, 11 m/d, and 22 m/d), the fast-sinking class contains the rest. We use $\Phi_{j,s}$ ($\Phi_{j,s} = \sum_{slow} \varnothing_{i,j}$) and $\Phi_{j,f}$ ($\Phi_{j,f} = \sum_{fast} \varnothing_{i,j}$) to represent interaction j in slow- and fast-sinking classes, respectively. By integrating Eq. (4), we obtained depth-integrated concentrations for each layer. For both slow- and fast-sinking classes, depth-integrated concentrations and flux differences at the upper and lower boundary of each layer are presented in Table 3. We get a set of linear equations by combining Eq. (3) and Eq. (4). Given a set of parameter values, the model concentrations are calculated by direct matrix inversion. We minimize the misfit between model and observed concentrations by optimizing a total of five rate constant parameters: aggregation (β), disaggregation (β_{-1}), Chl-a-to-pheopigment degradation (d_1), organic matter remineralization (d_2), and pheopigment remineralization (d_3). The estimation is achieved by minimizing the following objective function.

$$f(\mathbf{p}) = \Gamma \cdot (C(p)_m - \mathbf{C_o})' \sigma_d^{-1} (C(p)_m - \mathbf{C_o}) + \Lambda \cdot (\mathbf{p} - \mathbf{p_0})' \sigma_p^{-1} (\mathbf{p} - \mathbf{p_0}),$$
where $\mathbf{p} = \log([\beta, \beta_{-1}, d_1, d_2, d_3])$ (5)

The objective function corresponds to the negative logarithm of the posterior probability function. The right hand side of Eq. (5) has two terms corresponding to the log likelihood and the log prior. $\mathbf{C}(p)$ is a vector of model OM or pigment concentrations, which is an implicit function of the parameters of interest ($\mathbf{p}$). The subscripts m and o denote model predicted values and observed values, respectively. σ_d and σ_p are covariance matrix for data and parameter, respectively. Since the depth-integrated OM and pigment concentrations are several orders of magnitude different, to assign them comparable weights in the

Table 3

Depth-integrated OM and pigment concentrations, standard deviations (see text for detail), along with flux differences after separating them into slow- and fast-sinking classes. "Pheopigments" is the combination of *pheophorbide*, *pyropheophorbide*, and *pheophytin*.

	Chl a	Pheopigments	OM	Chl a	Pheopigments	OM
	Layer I (313–524 m) slow-sinking			Layer I (313–524 m) fast-sinking		
Concentration[a]	0.305	2.463	0.922	0.009	0.070	0.023
STD[a]	0.649	5.053	2.187	0.021	0.152	0.058
ΔFlux[b]	0.543	5.759	1.357	− 0.002	7.504	1.769
	Layer II (524–1918 m) slow-sinking			Layer II (524–1918 m) fast-sinking		
Concentration[a]	1.223	9.609	4.014	0.039	0.285	0.105
STD[a]	0.649	5.053	2.187	0.021	0.152	0.058
ΔFlux[b]	0.773	5.413	2.372	1.323	5.733	2.785

[a] Unit of pigments is µg/m², of OM is mg/m².
[b] Unit of pigments is µg/m²/y, of OM is mg/m²/y.

Table 4
The mean, exp($\mathbf{p_0}$), and variance, $\sigma_p{}^2$, for the prior probability distribution along with the most probable posterior estimates and their error bars that correspond to plus\minus one standard deviation of the posterior probability distribution. Because the prior is based on lognormal distributions the prior variances listed in this table are for the logarithm of the parameters. In addition, the prior variance gets rescaled by $1/\Lambda = 0.95$. Parameters estimated from pigments (this study) and Th (Wang et al., 2016) sediment trap data (unit: y^{-1}) are appended.

Parameters	exp($\mathbf{p_0}$)	$\sigma_p{}^2$	Sediment trap (using pigments)	Sediment trap (using Th)
β	5.4	4.01	$3.2_{-2.4}^{+9.9}$	0.07–1.88
β_{-1}	17.32	6.64	$149.9_{-99.6}^{+297.3}$	0.30–3.01
d1	0.32	2.98	$1.6_{-0.3}^{+0.4}$	–
d2	0.32	2.98	$1.5_{-0.4}^{+0.5}$	–
d3	0.32	2.98	$2.1_{-0.5}^{+0.7}$	–

objective function, we separated the data into six groups ($\text{Chl}_{f,s}$, $\text{pheo}_{f,s}$, and $\text{OM}_{f,s}$). Each group is normalized using their corresponding standard deviations, which is denoted as σ_d in Eq. (5) and is listed in Table 3. To keep parameter values positive, lognormal distribution is assumed for parameters. Γ and Λ are hyperparameters, which scale the data and prior precisions (inverse variance). $\mathbf{p_0}$ is a vector, whose elements are prior estimation of parameters that are shown in Table 4. Determination of Γ and Λ is based on the evidence approximation method described in MacKay (1992). In this method, the log evidence, log(Z), where Z is the marginal probability of the data after integrating the joint posterior for the data and the model parameters over all possible parameter values is maximized to select Γ and Λ. In other words the most probable hyperparameters values are used to determine the error bars for the model parameters. To make the integral over the parameters feasible, we approximate the posterior for the parameters as a multivariate Gaussian. Finding Γ and Λ is then equivalent to maximizing the following function

$$\log(Z(\Gamma, \Lambda)) = -f(\hat{\boldsymbol{p}}) - \frac{1}{2}\log(\det(\boldsymbol{A})) + \frac{k}{2}\log(\Lambda) + \frac{N}{2}\log(\Gamma) + \text{const.} \tag{6}$$

where $f(\hat{\boldsymbol{p}})$ is the value of objective function (5) evaluated at its minimum, i.e. at the most probable value of $\mathbf{p} \cdot \mathbf{A} \equiv \nabla\nabla f_{p=\hat{p}}$ is the Hessian matrix of second derivatives with respect to the parameters evaluated at the maximum of the posterior probability distribution. k is the number of parameters, and N is the number of data points. The constant term, being independent of Γ and Λ is irrelevant for the purpose of selecting the most probable hyper parameters.

We apply the same parameters to both layers to keep the model as parsimonious as possible. The optimization is based on a two level approach: The first level uses the methods described in Section 2.2 to estimate the parameters $\mathbf{p}$ by minimizing f defined in Eq. (5) for a given value of Γ and Λ. The second level, estimates Γ and Λ by maximizing log (Z) defined in Eq. (6). Because the model is not computationally expensive to evaluate, we optimized Γ and Λ using a simple grid search. The most probable Γ and Λ are then used to select the most probable $\mathbf{p}$. The error bars are computed by approximating the posterior with a Gaussian, i.e. by using the posterior covariance matrix $\Sigma = (-\nabla\nabla f_{p=\hat{p}})^{-1}$. The parameter estimates along with their error bars are listed in Table 4.

3. Results and discussion

3.1. Finite difference model and parameter recovery

To test the Bayesian method, we generated a set of synthetic data (as shown in Fig. 2) using a finite difference model, which we contaminated with random errors. Bayesian statistics were applied to the contaminated data to recover the parameters used in the finite difference model. To test the sensitivity of the recovered parameters to the data using the Bayesian method, we further contaminated the idealized data with noise of increasing variances from 0.05 to 0.5 (Recovery I–III in Table 1). As can be seen, the parameters recovered by the Bayesian method are in good agreement with the parameters used
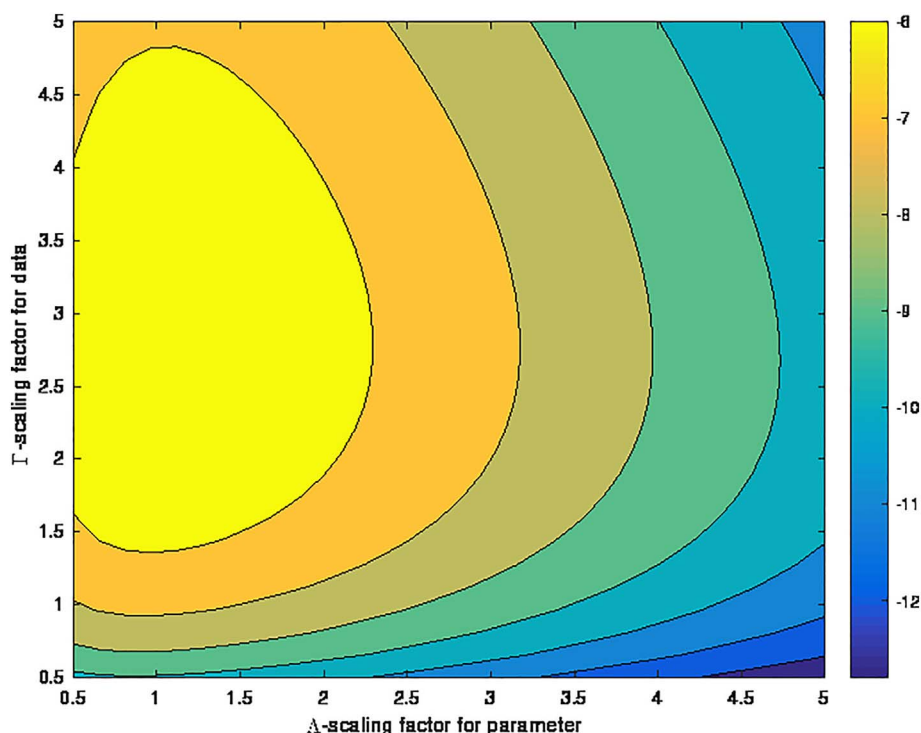
Fig. 3. Contour plot of the logarithm of the evidence, log(Z(Λ, Γ)) The maximum is located at $\Lambda = 1.05$ and $\Gamma = 2.81$.
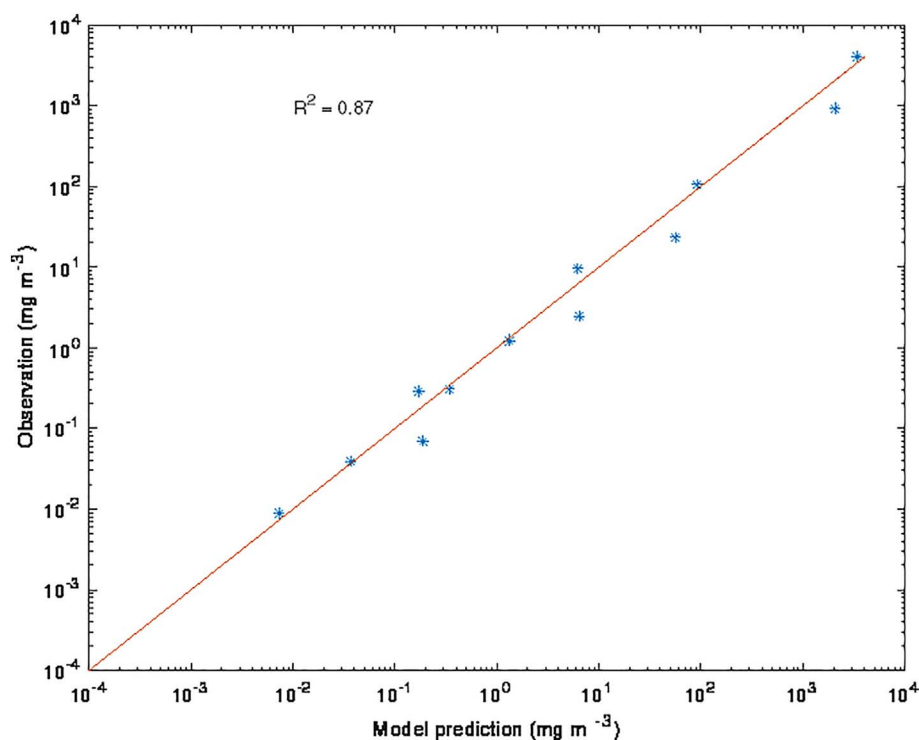
Fig. 4. Comparison of observed and model predicted POC/pigment concentrations.

to generate the data. The recovered parameters deviated more from the original parameters when higher variances were used to contaminate the data but, the estimated error bars also increased with increasing noise variance.

3.2. Two-layer model validation

By applying the Bayesian method to the SV trap measurement data as shown in Table 3, we obtained a set of most probable parameter values that along with the mean of the prior distribution are listed in Table 4. Fig. 3 shows the contour plot for finding Λ and Γ. The most probable value for Λ and Γ estimated by the model is 1.05 and 2.81, respectively. Fig. 4 shows model versus observation correlation. As can be seen, although OM and pigment concentrations have a range of five orders of magnitude, the two-layer model does a decent job of recovering the observed concentration, with a correlation coefficient of 0.87.

3.3. Aggregation and disaggregation rate constants estimated using chloropigments and thorium isotopes

Particle aggregation and disaggregation rate constants have been previously estimated using thorium isotope data from the 2005 MedFlux program and the maximum likelihood method by Wang et al. (2016). The parameter estimation based on the likelihood method used in Wang et al. (2016) effectively assumes flat priors for the parameters and the resulting parameter estimates can be interpreted as the most probable parameter values under the given assumptions. The Bayesian method used in this paper assumes a normal prior distribution, and the result of the analysis is interpreted is a posterior probability density that can be used in a straightforward way to obtain uncertainty estimates. The difference between likelihood and Bayesian methods leads to uncertainty estimates; in Wang et al. (2016) errors are the standard deviation of 100 runs with data contaminated with randomly distributed errors that are corresponding to measurement errors, whereas in this paper errors are obtained from parameter posterior density distributions.

Comparison with results using Th at other locations (Nozaki et al., 1987; Murnane et al., 1990; Clegg et al., 1991; Cochran et al., 1993; Murnane, 1994; Cochran et al., 2000) indicates that particle aggregation and disaggregation rate constants we estimated here using pigment tracers at the DYFAMED site (Wang et al., 2016) are very consistent with the reference ranges. However, Table 4 shows that aggregation rate constants calculated with pigment data from the same samples are tens of times higher than those estimated with thorium data, whereas disaggregation rate constants are hundreds of times higher in the current study than when estimated from thorium data.

These results led us to consider the differences in the way thorium and chlorophyll exist on and within particles. First, Chl is produced only in the euphotic zone by phytoplankton, so that its only source is from particles in the surface waters. The pheopigments are produced throughout the water column as Chl degrades. Since Chl a and its degradation products are an integral part of the organic matter in particles, and are not appreciably soluble in sea water, they remain on particles and do not participate in sorption processes to any great extent. In contrast, the thorium isotopes ^{234}Th and ^{230}Th, which were used in Wang et al. (2016), are produced by the decay of soluble ^{238}U and ^{234}U, respectively, in seawater, so are produced throughout the water column. Although initially dissolved, thorium is a surface-active element that sorbs to and desorbs from the particle surface (Moore and Millward, 1988). Clay, biogenic opal, manganese dioxide, and calcium carbonate may all sorb thorium (Geibert and Usbeck, 2004). Thorium isotopes produced in situ from U decay (e.g. ^{234,230}Th) can be incorporated inside a particle only when smaller particles aggregate and the "surface" is subsumed and mixed to some degree. Therefore, these two tracers undoubtedly record particle exchange in different ways.

If Th and Chl were truly representing the entire particle and were on the same particle, calculated aggregation rate constants should be similar. There are several possible reasons for the differences between the Th- and Chl-derived rate constants. As a particle reactive tracer, adsorption and desorption processes can dominate particle-thorium interactions, which may result in less accurate estimations of the particle aggregation and disaggregation rate constants than when using

chloropigments. This is because when first-order reaction kinetics are assumed, the contributions of aggregation and disaggregation in the steady state equation are small due to low particle concentration. This is not as important for pigments since they do not appreciably sorb and desorb. Thus, adsorption and desorption processes, which are much larger than aggregation, could dominate due to high dissolved thorium concentrations, and thus affect estimates of aggregation and disaggregation rate constants.

However, although both Th and Chl are present on both large and small particles, most likely they are present in different proportions in those particles. Chl is probably transported more with rapidly settling aggregates, whereas Th may be transported more by smaller particles. The surface area of the smaller particles is proportionately larger, so Th can continually sorb-desorb in interaction with the larger dissolved pool of Th. So neither tracer tracks "particles" perfectly. We don't know why the pigment-derived rate constants are so much higher than the Th-derived constants, other than being due to the difference in how they are packaged within the particle, but this is a topic for further research. Because there are a multitude of organic compounds on particles, it may be possible to use our modeling approach with other organic compounds with different properties.

Rather than their absolute amounts, it might be more useful to look at the ratio of disaggregation to aggregation rate constants, ~47 for Chl and ~4 for Th, which both indicate more disaggregation than aggregation at this depth. Thus these ratios are both consistent with higher abundance of "sticky" material (e.g., transparent exopolymer particles, or TEP) in the surface waters that would result in aggregation; but since TEP concentrations decrease with depth below the euphotic zone in this area (Ortega-Retuerta et al., 2010), aggregation of OM would be low below 300 m, the depth of our shallowest trap. There are other complicating factors using either Th or chloropigments to calculate process rate constants. Radioactive decay and production rates are known for Th isotopes, while Chl a degrade to pheopigments and to colorless products at a variety of poorly known rates. If we consider that Chl a degrades to colorless components, the aggregation rate constants derived here are underestimated and disaggregation rate constants are overestimated in the two-layer model. This is because Chl a degradation is underestimated and pheopigment production is overestimated in slow-sinking classes, resulting in higher Chl a and higher pheopigments, which are compensated by a lower aggregation rate constant and a higher disaggregation rate constant in the balance equations. Particle aggregation rate constants obtained from chloropigment data may also be biased because pigments are a small part of the POC and thus may trace only phytoplankton-derived part of the bulk particles.

Differences between rate constants determined in the current study and studies in other areas could be due to several factors. Geographical or seasonal variations may alter aggregation rate constants; the area of this study was in the Mediterranean Sea and the areas studied in most of the references were in more oligotrophic areas of the Pacific or western Atlantic. According to Murnane (1994), aggregation rate constants estimated at different locations can differ by 2 orders of magnitude. According to Abramson et al. (2010), the extent of particle exchange could be distinctly different if sampling seasons are different. In spring of 2003 when the major phytoplankton bloom occurred, there appeared to be almost no particle exchange, while in summer, exchange was clearly shown to be present.

3.4. Chl a and OM degradation rate constants

Marine pigment degradation rate calculations have been made for coastal surface sediments but not to our knowledge for sinking particles. Sediment material will undoubtedly be somewhat more decomposed than trap material. Sun et al. (1993) investigated Chl-a degradation in coastal marine sediments by applying the Multi-G model, in which organic matter is assumed to have different pools with different labilities and different decomposition rate constants (Westrich and Berner, 1984; Whelan and Farrington, 2013). Sun et al. (1993) concluded that the first-order degradation rate constant of labile Chl a, which constituted about 75% of total Chl a, was about 0.25 d^{-1} (90 y^{-1}), and for refractory Chl a ranged from 0.03 to 0.09 d^{-1} (10–30 y^{-1}) for oxic sediments. Stephens et al. (1997) also reported first-order reaction rate constants for Chl a that ranged from 1 to 75 y^{-1} in sediment sampled at four abyssal sites in the equatorial Pacific. The rate constants found in our study ($1.6_{-0.3}^{+0.4}$ y^{-1}) are at the lower end of the above reported ranges. Chl-a degradation as defined in this study included only degradation into pheopigments. Pigments can also be degraded into colorless products, and thus our calculated degradation rate constant is an under-estimate compared to total degradation. Considering the different environments studied, the much lower concentrations of organic matter in the water column than in sediments, and the fact that we looked only at degradation into pheopigments, the lower Chl-a degradation rate constants found in our study appear reasonable.

Westrich and Berner (1984) reported that the degradation rate constants of labile organic matter in coastal sediment is 24 ± 4 y^{-1}, while that of less reactive POC or TOC is 1.4 ± 0.7 y^{-1}. Our estimation that POC degradation rate constant of $1.5_{-0.4}^{+0.5}$ y^{-1}, is in good agreement with their values, since at the depth of 313 m, much of the labile POC has degraded; the estimated rate constants at our study depths should be for less reactive POC. Comparison of our POC degradation rate constants with the respiration rate constants obtained using thorium tracers (1.74×10^{-3} y^{-1} between 313 and 524 m and 0.50 y^{-1} between 524 and 1918 m in Wang et al., 2016) shows that the POC degradation rate constants here are higher. This is because the "respiration" rate constants in Wang et al. (2016) are a weighted average that includes both mineral dissolution and organic matter respiration. In addition, the pheopigment respiration rate constant and Chl-a degradation rate constant estimated in this study are higher than the POC remineralization rate constant, which is consistent with the view that pigment loss is somewhat faster than total OM loss (Lee et al., 2000).

3.5. Process contributions

Abramson et al. (2010) found very little evidence for particle exchange in the high-flux spring (2003 and 2005), but considerable in the low-flux summer (2003). We cannot directly compare our results with those of Abramson et al. (2010) because they used in-situ pump data for the "slow-sinking" particles in their analysis, while we used two different velocity classes of sediment trap data. In addition, in 2005, only spring samples were collected and the pigment flux peak caused by the spring bloom was about 2 weeks later and half as large as in 2003. However, for the purposes of a comparison, we made the assumption that particles in the slow-sinking class (< 49 m/d) of our two-layer model were similar to the particles sampled by large volume in-situ pumps in Abramson et al. (2010), and that particles in the fast-sinking class (≥ 49 m/d) were similar to the particles sampled by TS sediment traps. This assumption is supported by the principal component analysis of the 2005 organic compound data from the same samples by Abramson et al. (2010) that shows the greater similarity of sediment trap particle composition with pump-collected large particles (> 70 μm) than with that of pump-collected small (1–70 μm) particles. We then calculated contributions to the flux changes from the various processes by multiplying rate constants (from Table 4) times corresponding model concentrations. As can been seen from the results in Table 5, particle aggregation and disaggregation rates are more similar than the rate constants. Whereas the particle disaggregation rate constant was 46 times higher than the aggregation rate constant, the disaggregation rate was little different from the aggregation rate. This seems inconsistent with the specific compound

Table 5
Contribution of each process. Negative values indicate sinks. Positive values are sources. Unit of pigments is μg/m²/y, of POC is mg/m²/y.

Process	Layer I 313–524 m		Layer II 524–1918 m	
	Fast-sinking	Slow-sinking	Fast-sinking	Slow-sinking
Aggregation (Chl *a*)	1.155	− 1.155	4.471	− 4.471
Disaggregation (Chl *a*)	− 1.153	1.154	− 5.794	5.794
Chl-*a* degradation	–	− 0.541	–	− 2.096
Δ*f* (Chl *a*)	− 0.002	0.543	1.323	0.773
Aggregation (pheo-)	21.744	− 21.744	20.859	− 20.859
Disaggregation (pheo-)	− 29.248	29.248	− 26.592	26.592
Degradation (pheo-)	–	− 13.804	–	− 13.242
Chl-*a* degradation	–	0.541	–	2.096
Δ*f* (pheo-)	7.504	5.759	5.733	5.413
Aggregation (OM)	6.97	− 6.97	11.47	− 11.47
Disaggregation (OM)	− 8.74	8.74	− 14.26	14.26
Degradation (OM)	–	-3.13	–	− 5.16
Δ*f*(OM)	1.77	1.36	2.78	2.37

data shown in Abramson et al. (2010) showing the difference in composition between the different particle fractions. Disaggregation of the fast-sinking particles forms a major source of pheopigments to the slow-sinking class. Thus, pheopigments in slow-sinking particles are derived mainly from the disaggregation of fast-sinking particles. Also, disaggregation is the main sink of fast-sinking organic matter, which is in good agreement with the results of Abramson et al. (2010; Fig. 6 therein). We cannot examine how aggregation and disaggregation changed seasonally as in Abramson et al. (2010), because SV sediment traps integrate particles over the entire deployment period.

It is interesting to compare a similar approach that Wang et al. (2016) used to calculate particle aggregation and disaggregation rates using Th activities (see their Table 3). They multiplied their calculated Th rate constants times the measured Th activity and found that for both ²³⁰Th and ²³⁴Th, aggregation rates of slow-sinking particles to fast-sinking particles were orders of magnitude higher than disaggregation rates. As for the pigments, this is opposite to the rate constant estimates. This raises the question of which parameters are most important in studies of particle dynamics. It will depend on the question being asked as to whether the rates or rate constants are more useful.

4. Conclusions

Parameters estimated using pigment tracers and the two-layer model are in the range of parameters estimated using thorium tracers. However, comparison to our previous study using thorium tracers, which are from the same samples, reveals different characteristics between the two kinds of tracers. We show here that particulate pigments cycle differently than particulate thorium, as reflected by the different optimal parameters. Thorium and other surface-active elements would behave very differently as they are adsorbing and desorbing from the surface. This study shows that care should be taken to consider all components of marine particles when calculating rates of biogeochemical processes like aggregation, disaggregation and remineralization. Multiple tracers should be used to obtain a comprehensive picture of particle exchange processes. The model clearly illustrates the difference between Chl *a* and Th due to different supply mechanisms and fates in the water column, and therefore has the potential to further explore particle dynamics as well as address the fate of individual particle compounds.

Acknowledgements

References

Abramson, L., Lee, C., Liu, Z., Wakeham, S.G., Szlosek, J., 2010. Exchange between suspended and sinking particles in the northwest Mediterranean as inferred from the organic composition of in situ pump and sediment trap samples. Limnol. Oceanogr. 55, 725–739.

Armstrong, R.A., Peterson, M.L., Lee, C., Wakeham, S.G., 2009. Settling velocity spectra and the ballast ratio hypothesis. Deep Sea Res. II 56, 1470–1478.

Clegg, S.L., Bacon, M., Whitfield, M., 1991. Application of a generalized scavenging model to thorium isotope and particle data at equatorial and high-latitude sites in the Pacific Ocean. J. Geophys. Res.: Oceans 96 (C11), 20655–20670.

Cochran, J.K., Buesseler, K.O., Bacon, M.P., Livingston, H.D., 1993. Thorium isotopes as indicators of particle dynamics in the upper ocean: results from the JGOFS North Atlantic bloom experiment. Deep Sea Res. I 40, 1569–1595.

Cochran, J., Buesseler, K., Bacon, M., Wang, H., Hirschberg, D., Ball, L., Andrews, J., Crossin, G., Fleer, A., 2000. Short-lived thorium isotopes (²³⁴Th, ²²⁸Th) as indicators of POC export and particle cycling in the Ross sea Southern Ocean. Deep Sea Res. II 47, 3451–3490.

Geibert, W., Usbeck, R., 2004. Adsorption of thorium and protactinium onto different particle types: experimental findings. Geochim. Cosmochim. Acta 68, 1489–1501.

Hill, P.S., 1998. Controls on floc size in the sea. Oceanography 11, 13–18.

Honjo, S., 1980. Material fluxes and modes of sedimentation in the mesopelagic and bathypelagic zones. J. Mar. Res. 38, 53–97.

Lee, C., Wakeham, S.G., 1988. Organic Matter in Seawater: Biogeochemical Processes. Academic Press.

Lee, C., Wakeham, S.G., Hedges, J.I., 2000. Composition and flux of particulate amino acids and chloropigments in equatorial Pacific seawater and sediments. Deep Sea Res. I 47, 1535–1568.

Lee, C., Armstrong, R.A., Cochran, J.K., Engel, A., Fowler, S.W., Goutx, M., Masqué, P., Miquel, J.C., Peterson, M., Tamburini, C., Wakeham, S., 2009a. Medflux: investigations of particle flux in the twilight zone. Deep Sea Res. II 56, 1363–1368.

Lee, C., Peterson, M.L., Wakeham, S.G., Armstrong, R.A., Cochran, J.K., Miquel, J.C., Fowler, S.W., Hirschberg, D., Beck, A., Xue, J., 2009b. Particulate organic matter and ballast fluxes measured using time-series and settling velocity sediment traps in the northwestern Mediterranean Sea. Deep Sea Res. II 56, 1420–1436.

MacKay, D.J., 1992. Bayesian interpolation. Neural Comput. 4, 415–447.

Marty, J.-C., 2002. The DYFAMED time-series program (French-JGOFS). Deep Sea Res. II 49, 1963–1964.

Marty, J.-C., Chiavérini, J., Pizay, M.-D., Avril, B., 2002. Seasonal and interannual dynamics of nutrients and phytoplankton pigments in the western Mediterranean Sea at the DYFAMED time-series station (1991–1999). Deep-Sea Res. II 49, 1965–1985.

McCave, I., 1975. Vertical flux of particles in the ocean. Deep-Sea Res. 22, 491–502.

Moore, R., Millward, G., 1988. The kinetics of reversible Th reactions with marine particles. Geochim. Cosmochim. Acta 52, 113–118.

Murnane, R.J., 1994. Determination of thorium and particulate matter cycling parameters at station P: a reanalysis and comparison of least squares techniques. J. Geophys. Res.: Oceans 99 (C2), 3393–3405.

Murnane, R.J., Sarmiento, J.L., Bacon, M.P., 1990. Thorium isotopes, particle cycling models, and inverse calculations of model rate constants. J. Geophys. Res.: Oceans 95 (C9), 16195–16206.

Murnane, R., Cochran, J., Sarmiento, J., 1994. Estimates of particle-and thorium-cycling

rates in the northwest Atlantic Ocean. J. Geophys. Res.: Oceans 99 (C2), 3373–3392.

Murnane, R., Cochran, J., Buesseler, K., Bacon, M., 1996. Least-squares estimates of thorium, particle, and nutrient cycling rate constants from the JGOFS North Atlantic bloom experiment. Deep Sea Res. I 43, 239–258.

Nozaki, Y., Yang, H.-S., Yamada, M., 1987. Scavenging of thorium in the ocean. J. Geophys. Res.: Oceans 92 (C1), 772–778.

Ortega-Retuerta, E., Duarte, C.M., Reche, I., 2010. Significance of bacterial activity for the distribution and dynamics of transparent exopolymer particles in the Mediterranean Sea. Microb. Ecol. 59, 808–818.

Kriest, I., Oschlies, A., 2008. On the treatment of particulate organic matter sinking in large-scale models of marine biogeochemical cycles. Biogeosciences 5, 55–72.

Peterson, M., Hernes, P., Thoreson, D., Hedges, J., Lee, C., Wakeham, S., 1993. Field evaluation of a valved sediment trap. Limnol. Oceanogr. 38, 1741–1761.

Peterson, M.L., Wakeham, S.G., Lee, C., Askea, M.A., Miquel, J.C., 2005. Novel techniques for collection of sinking particles in the ocean and determining their settling rates. Limnol. Oceanogr.: Methods 3, 520–532.

Peterson, M.L., Fabres, J., Wakeham, S.G., Lee, C., Alonso, I.J., Miquel, J.C., 2009. Sampling the vertical particle flux in the upper water column using a large diameter free-drifting NetTrap adapted to an Indented Rotating Sphere sediment trap. Deep Sea Res. II 56, 1547–1557.

Shuman, F.R., Lorenzen, C.J., 1975. Quantitative degradation of chlorophyll by a marine herbivore. Limnol. Oceanogr. 20, 580–586.

Sivia, D.S., Skilling, J., 2006. Data Analysis-A Bayesian tutorial. Oxford University Press.

Stephens, M.P., Kadko, D.C., Smith, C.R., Latasa, M., 1997. Chlorophyll-a and

pheopigments as tracers of labile organic carbon at the central equatorial Pacific seafloor. Geochim. Cosmochim. Acta 61, 4605–4619.

Sun, M.-Y., Lee, C., Aller, R.C., 1993. Laboratory studies of oxic and anoxic degradation of chlorophyll-a in Long Island sound sediments. Geochim. Cosmochim. Acta 57, 147–157.

Szymczak-Zy la, M., Kowalewska, G., Louda, J.W., 2008. The influence of microorganisms on chlorophyll *a* degradation in the marine environment. Limnol. Oceanogr. 53, 851–862.

Teng, Y.-C., Primeau, F.W., Moore, J.K., Lomas, M.W., Martiny, A.C., 2014. Global-scale variations of the ratios of carbon to phosphorus in exported marine organic matter. Nat. Geosci. 7, 895–898.

Wakeham, S., Lee, C., Peterson, M., Liu, Z., Szlosek, J., Putnam, I., Xue, J., 2008. Organic compound composition and fluxes in the twilight zone - time series and settling velocity sediment traps during MEDFLUX. Deep-Sea Res. II 56, 1437–1453.

Wang, W.L., Armstrong, R.A., Cochran, J.K., Heilbrun, C., 2016. ^{230}Th and ^{234}Th as coupled tracers of particle cycling in the ocean: a maximum likelihood approach. Deep-Sea Res. I 111, 61–70.

Welschmeyer, N.A., Lorenzen, C.J., 1985. Chlorophyll budgets: zooplankton grazing and phytoplankton growth in a temperate fjord and the central Pacific gyres. Limnol. Oceanogr. 30, 1–21.

Westrich, J.T., Berner, R.A., 1984. The role of sedimentary organic matter in bacterial sulfate reduction: the G model tested. Limnol. Oceanogr. 29, 236–249.

Whelan, J.K., Farrington, J.W., 2013. Organic Matter: Productivity, Accumulation, and Preservation in Recent and Ancient Sediments. Columbia University Press.